CRYSTAL GROWTH & DESIGN

pubs.acs.org/crystal

Article

Amorphous Calcium–Magnesium Carbonate (ACMC) Accelerates Dolomitization at Room Temperature under Abiotic Conditions

German Montes-Hernandez,* François Renard, Anne-Line Auzende, and Nathaniel Findling

Cite This: *Cryst. Growth Des.* 2020, 20, 1434–1441

Read Online

ACCESS | Metrics & More | Article Recommendations | Supporting Information

ABSTRACT: The challenge to produce dolomite $CaMg(CO_3)_2$ at low temperature (20–35 °C) over laboratory time scales so far has remained unsuccessful, which has led to long-lasting scientific debates in the last two centuries. This mineral exerts a major control on the natural carbon dioxide sequestration into various sedimentary, basaltic, and mantellic rocks. The present study reports on specific abiotic conditions that allow the precipitation of disordered dolomite, high Mg calcite, and high Ca magnesite at room temperature over time scales of hours to days. Here we show that an amorphous calcium magnesium carbonate (ACMC) phase accelerates dolomitization at room temperature. ACMC is initially precipitated by mixing a carbonate (HCO_3^-/CO_3^{2-} = 1; pH ~10.3 ≈ pK_{a2}) alkaline solution with a Mg-Ca ionic solution (Mg molar fraction between 0 and 1). Then, time-resolved in situ Raman spectroscopy monitored the transformation of ACMC into Mg-rich carbonate minerals. The initial Mg molar fraction controlled both the reaction mechanism (e.g., nature of transient crystalline phases) and the kinetics. Nanosized crystallites with short-range order, called disordered dolomite $CaMg(CO_3)_2$, precipitated following a complex reaction pathway. First, nesquehonite ($MgCO_3{\cdot}3H_2O$: nucleation time 2.5 h) and then disordered dolomite ($CaMg(CO_3)_2$: nucleation time 3.2 h) followed by monohydrocalcite ($CaCO_3{\cdot}H_2O$: nucleation time 3.4 h) formed from ACMC transformation. Nesquehonite and monohydrocalcite are transient phases that nourish the slow precipitation of disordered dolomite, which reached a spectral equilibrium after 7 days of reaction. The direct transformation of ACMC into disordered dolomite was also measured. Our experimental results demonstrate that disordered dolomite precipitates at room temperature when an ideal Mg/Ca ratio, high carbonate alkalinity, and high ionic concentration are reached in abiotic systems. This result suggests the possibility of a physicochemical rather than biotic control on the formation of disordered dolomite at low temperature in several geosystems.

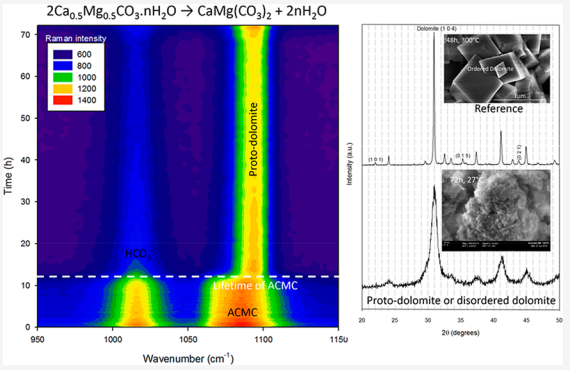

1. INTRODUCTION

The precipitation kinetics and formation mechanism of dolomite, $CaMg(CO_3)_2$, have been widely studied, and controversial claims have been reported in the past two centuries.[1] The abiotic precipitation of dolomite at ambient temperature (~25 °C) is virtually impossible within typical laboratory experimental time scales.[2−5] This difficulty is interpreted to originate from the strongly bonded solvation shells of magnesium ions in aqueous media.[2] The dehydration of Mg ions is significantly facilitated by bacterial activity, including exopolymeric substances, and organic functionalized surfaces.[6,7] Therefore, several studies have claimed that dolomite may precipitate in bioassisted systems under ambient laboratory conditions.[6−12] Therefore, both textural and crystallographic characterization, reaction mechanism, and kinetics studies of dolomite precipitation at ambient/low temperature remain exciting scientific challenges for geochemists and mineralogists.[13−17]

In addition, the effect of Mg hydration might not be the only factor of inhibition of dolomite formation at room temperature. Recent studies claimed that a more intrinsic crystallization barrier and the influence of fluid chemistry (e.g., relative size of the cations in solution) may prevent the formation of long-range ordered crystallographic structures in dolomite under ambient conditions.[3−5] Lippmann[18] described specific superstructures, called ordering reflections, in the X-ray diffraction patterns of dolomite that were related to the regular alternation of monolayers of Ca and Mg oriented perpendicular to the *c* axis of dolomite crystals. This organization indicates an equal Mg and Ca composition in the structure at the crystal scale. In natural dolomites, structural imperfections are frequently measured and, sometimes, nanometer-sized crystallites with short-range order may be expected.[1] In this last case, the term disordered dolomite (also called protodolomite) is used because the superstructure-ordering reflections,

Received: July 29, 2019
Revised: January 24, 2020
Published: January 27, 2020

https://dx.doi.org/10.1021/acs.cgd.9b01005
Cryst. Growth Des. 2020, 20, 1434–1441

Table 1. List of Experiments with Time-Lapse Raman Spectroscopy for Precipitation of Disordered Dolomite at Room Temperature and Influence of Mg Molar Ratio[a]

expt	temp (°C)	Mg molar fraction	expt duration (days)	lifetime of ACMC	mineral transient phase(s)	final mineral phase(s)
1	27	0.75	3	10 h	none	disordered dolomite[b]
2	31	0.75	7	2.5 h	nesquehonite, monohydrocalcite	disordered dolomite[b]
3	31	0.75	7	2.3 h	nesquehonite, monohydrocalcite	disordered dolomite
4	30	0.75	10	1.9 h	nesquehonite, monohydrocalcite	disordered dolomite
5	28	0	1	0.75 min	vaterite	calcite[b]
6	28	0.05	1	1.75 min	vaterite	calcite[b]
7	29	0.20	2	3 min	vaterite	low Mg calcite[b]
8	27	0.5	2	3 min	none	high Mg calcite[b]
9	28	0.6	2	30 min	none	high Mg calcite[b]
10	29	0.9	2	4.5 h	monohydrocalcite	disordered dolomite,[b] dypingite[b]
11	28	1	3	2 h	none	dypingite

[a]A constant carbonate alkalinity of HCO_3^-/CO_3^{2-} = 1 (0.5 M) and a total cationic (Mg-Ca) concentration of 0.5 M were imposed. [b]These phases were also characterized by powder X-ray diffraction.

corresponding to the peaks (101), (015), and (021) in X-ray diffraction patterns, are not detected.[13,19]

The present study demonstrates that an amorphous calcium−magnesium carbonate phase (ACMC) accelerates the dolomitization process at room temperature under abiotic conditions. Herein, an ACMC phase was instantaneously precipitated by using concentrated ionic solutions (HCO_3^-/CO_3^{2-} solution and Mg^{2+}/Ca^{2+} solution interactions). Then, the persistence time or lifetime (i.e., the duration until ACMC starts transforming) and transformation of ACMC into new minerals in the interacting solutions were monitored in real time by using dynamic Raman spectroscopy.[20] We also investigated the effect of the Mg molar fraction with respect to Ca in solution. This parameter controls the amount of Mg that can be incorporated into the carbonate crystal lattice and the nature of transient carbonate phases, allowing the precipitation of calcite (Mg/(Mg + Ca) = 0), low Mg calcite (Mg/(Mg + Ca)<10%), high Mg calcite (10% < Mg/(Mg + Ca) < 45%), disordered dolomite (45% < Mg/(Mg + Ca) ≤ 55%), and high Ca magnesite (Mg/(Mg + Ca) > 60%), as reported in the literature (e.g. refs 21−25).

High Mg calcite and disordered dolomite precipitation at room temperature are frequently related to biomineralization processes, as observed in corals, seashells, and many other invertebrates or observed in laboratory experiments under biotic conditions.[16,21] The present experimental study demonstrates that disordered dolomite, $CaMg(CO_3)_2$, can precipitate at low temperature when an ideal Mg/Ca ratio, high carbonate alkalinity (HCO_3^-/CO_3^{2-} coexistence), and high ionic concentration are reached in abiotic or biotic systems. Herein, the formation of an amorphous phase plays a significant role in producing disordered dolomite

2. MATERIALS AND METHODS

2.1. Disordered Dolomite $CaMg(CO_3)_2$ Formation at Room Temperature. The conditions to precipitate disordered dolomite at room temperature (27−31 °C) were the following: 100 mL of $NaHCO_3$ (1 M) and 100 mL of Na_2CO_3 (1 M) were placed into a Hastelloy C22 reactor (Parr, total internal volume of 600 mL) coupled with a Raman probe immerged into a solution/suspension in order to monitor precipitating carbonate particles and aqueous carbonate species in real time. This experimental setup was reported previously by the Montes-Hernandez group.[20] Raman spectra were collected with a Raman RXN1 instrument from Kaiser Optical Systems with an exposure time of 3 s and averaged over three scans.

The carbonate speciation in initial solution was verified by Raman spectroscopy before the injection of Ca-Mg solution (HCO_3^- peaking at 1016 cm^{-1} and CO_3^{2-} peaking at 1066 cm^{-1}; see Figure S1A). This carbonate alkaline solution was immediately dispersed by mechanical agitation (400 rpm) before 200 mL of a Ca-Mg solution (Mg molar fraction of 0.75 and Mg concentration of 0.375 M) was injected for about 1−2 min with a syringe. Following this injection step, the carbonate speciation and precipitated particles (i.e., transformation of amorphous calcium−magnesium carbonate ACMC into carbonate crystalline phases) were monitored by Raman spectroscopy for 3−7 days, with an acquisition frequency of one Raman spectra every 1 min during the first 3 h and every 5 or 10 min in the remaining time.

Selected Raman peaks corresponding to identified mineral phases (see Table S1) were fitted by using simple or combined Gaussian model in order to estimate both the full width at half-maximum (fwhm) and integrated peak area as a function of time (Movie S1). This calculation provided the peak decomposition necessary to propose relevant reaction mechanisms and to quantify the kinetics of precipitation of disordered dolomite ($MgCa(CO_3)_2$).

2.2. Role of Mg Molar Fraction. The persistence time of amorphous calcium−magnesium carbonate (ACMC) and its transformation into crystalline carbonate phases in the interacting solutions were measured as a function of Mg molar fraction (Mg molar fraction = $V_{Mg}/(V_{Mg} + V_{Ca})$) that was varied between 0 and 1 (experiments 5−11 in Table 1). Herein, the persistence time, also called lifetime, is defined as the duration over which ACMC is the only precipitate phase present in the suspension before starting to transform into crystalline carbonate phases. We define the nucleation time of each crystalline phase as the time at which this mineral is detected by Raman spectroscopy. These experiments were performed by following the same protocol described in section 2.1, except for the added volume of Ca and Mg solutions that was adjusted for each investigated Mg molar fraction. Table 1 summarizes all precipitation experiments performed in this study; each experiment was repeated at least twice to verify the reproducibility of the results.

2.3. Ex Situ Characterization of Precipitates. At the end of each experiment, the solid product was recovered by centrifugation and washed twice with ultrapure water and once with ethanol. Then, it was dried under a laminar flow of air at 20 °C for 48 h. The dry solid products were stored in plastic flasks for subsequent characterization of selected samples by field emission gun scanning electron microscopy (FESEM), transmission electron microscopy (TEM), and powder X-ray diffraction (XRD).

Powder XRD spectra were acquired using a Siemens D5000 diffractometer in Bragg−Brentano geometry, equipped with a $\theta-\theta$ goniometer with a rotating sample holder. Diffraction patterns were collected using Cu Kα_1 ($\lambda_{K\alpha_1}$ = 1.5406 Å) and Cu Kα_2 ($\lambda_{K\alpha_2}$ = 1.5444 Å) radiation in the range 2θ = 10−70°, with a step size of 0.04° and a counting time of 6 s per step. For high-resolution imaging, the solid products were dispersed by ultrasonic treatment in absolute ethanol

https://dx.doi.org/10.1021/acs.cgd.9b01005
Cryst. Growth Des. 2020, 20, 1434−1441

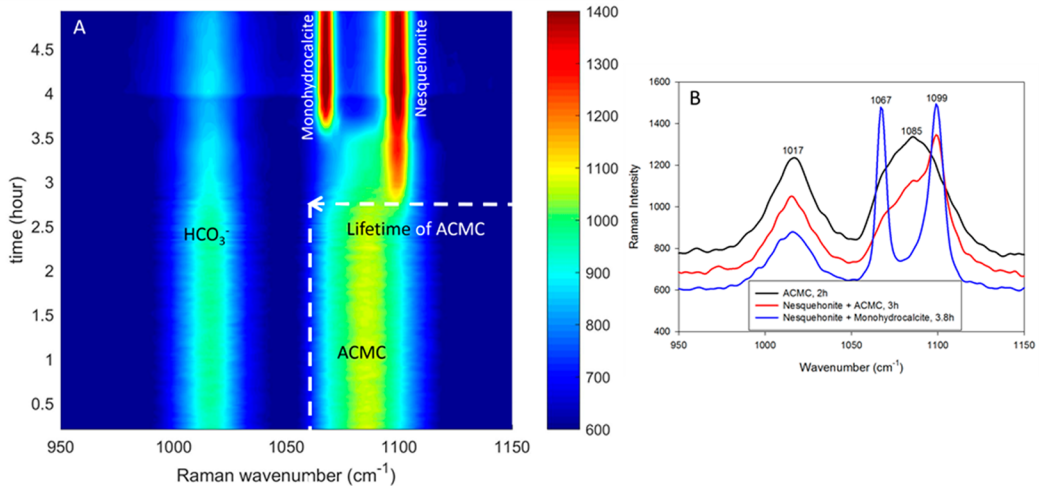

Figure 1. Time-lapse Raman spectroscopy monitoring of amorphous calcium−magnesium carbonate (ACMC) transformation into crystalline phases during the first 4 h of experiment 2 (Table 1). The lifetime of ACMC and positions of crystalline phases are indicated.

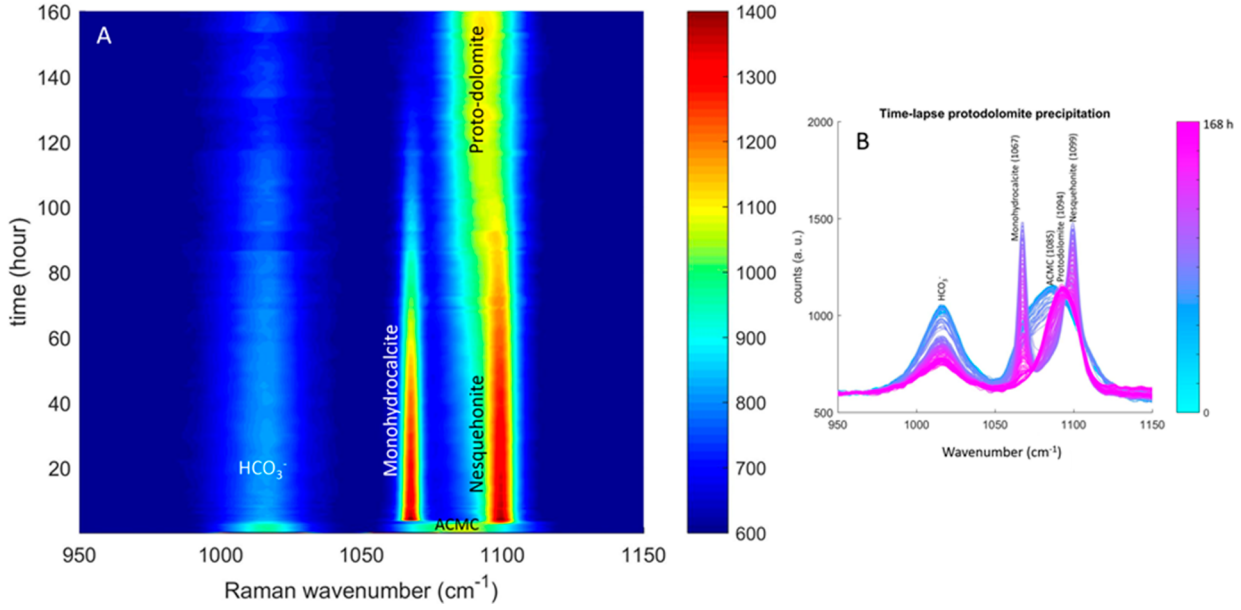

Figure 2. Time-lapse Raman spectroscopy monitoring of the formation of disordered dolomite from ACMC in experiment 2 (Table 1): (left) evolution of the two transient phases, nesquehonite and monohydrocalcite; (right) time-lapse evolution of the main peaks.

for 5 min. Two droplets of the suspension were then deposited directly on an aluminum support and coated with gold−platinum. The powder was imaged using a Zeiss Ultra 55 FESEM with a maximum spatial resolution of approximately 1 nm at 15 kV. In addition, recovered solid products from experiments 1 and 2 (Table 1) were shaken in ethanol for a short time in order to separate the aggregates without any additional treatment. One droplet of the suspension was deposited on a perforated carbon foil and placed on a conventional copper microgrid for further observations with a JEOL 2100F transmission electron microscope (TEM) operating at 200 kV, equipped with a field emission gun and a high-resolution pole piece achieving a point-to-point resolution of 1.8 Å. Chemical analyses at selected points on the sample were performed by electron dispersive spectroscopy (EDS).

3. RESULTS

3.1. Precipitation of Disordered Dolomite at Room Temperature: Reaction Mechanism and Kinetics. Concentrated ionic solutions were chosen to produce an amorphous calcium−magnesium carbonate (ACMC) phase. Our in situ Raman spectroscopy data confirmed the instantaneous formation of ACMC when an alkaline carbonate solution (HCO_3^-/CO_3^{2-} = 1) was mixed with Mg-Ca solution (Mg molar fraction 0.75), as displayed for three experiments in Figure S1B. The precipitated ACMC ($Ca_{0.5}Mg_{0.5}CO_3{\cdot}nH_2O$) is characterized by a broad Raman peak at 1085 cm^{-1}, shifted 6 cm^{-1} away and broader with respect to the peak of amorphous calcium carbonate (ACC: $CaCO_3{\cdot}nH_2O$) at 1079 cm^{-1} (this study), close to the value of 1080 cm^{-1} reported in other studies (e.g. refs 26 and 27). Time-resolved Raman spectroscopy shows that ACMC starts transforming into crystalline phases after about 2.5 h of reaction. Nesquehonite ($MgCO_3{\cdot}3H_2O$) is the first detected phase, with a peak at 1099 cm^{-1} and a nucleation time of 2.5 h, followed by monohydrocalcite ($CaCO_3{\cdot}H_2O$), with a peak at 1067 cm^{-1} and a nucleation time of 3.3 h (Figure 1). All phases detected in the time-resolved Raman spectroscopy measurements are summarized

https://dx.doi.org/10.1021/acs.cgd.9b01005
Cryst. Growth Des. 2020, 20, 1434−1441

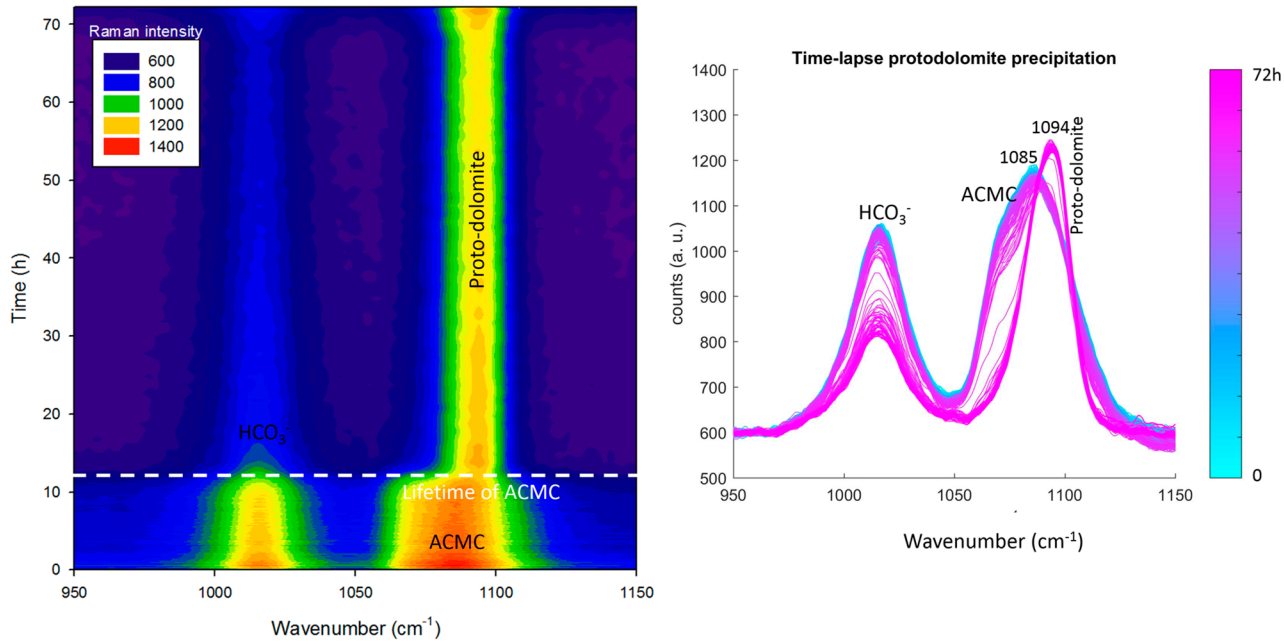

Figure 3. (left) Time-lapse Raman spectroscopy monitoring of the formation of disordered dolomite from direct transformation of ACMC in experiment 1 (Table 1). (right) Time-lapse evolution of the main peaks.

in Table S1, and their Raman feature assignation is supported by previous studies that systematically used ex situ Raman spectroscopy of powdered samples. Nesquehonite and monohydrocalcite are transient phases: i.e., their slow concurrent dissolution allows the continuous precipitation of disordered dolomite with a Raman peak at 1094 cm^{-1} (Figure 2). The broad feature of the main peak and low Raman signal in lattice mode at 300 cm^{-1} suggest the presence of nanosized crystals, as confirmed by FESEM images that reveal crystallites with size in the range 20−80 nm and formation of irregular aggregates (Figure S2). Herein, we suggest that this phase is a disordered dolomite, i.e. short-range order formation of nanosized crystallites, because the superstructure-ordering reflections ((101), (015), and (021)) are not detected in our laboratory X-ray powder diffraction, despite an ideal atomic composition (Mg/Ca = 1) (Figure S3).

Movie S1 displays the time evolution of the peaks of the main mineral phases during experiment 2 (Table 1), leading to the formation of disordered dolomite, including the evolution of ACMC, nesquehonite, and monohydrocalcite. The surface areas of the peaks corresponding to these four phases evolve as a function of time and are used here as proxies to measure the relative concentrations of these components in the suspension (Figure S4).

From these time-resolved Raman measurements and spectra analyses (Figures 1 and 2 and Figure S4), the following reactions are proposed, which summarize the mechanism for disordered dolomite formation.

Nesquehonite formation:

$$2Ca_{0.5}Mg_{0.5}CO_3{\cdot}nH_2O + 3H_2O \rightarrow MgCO_3{\cdot}3H_2O + CaCO_3{\cdot}nH_2O + nH_2O \quad (1)$$

Monohydrocalcite formation:

$$CaCO_3{\cdot}nH_2O + H_2O \rightarrow CaCO_3{\cdot}H_2O + nH_2O \quad (2)$$

Formation of disordered dolomite via concurrent dissolution of transient phases:

$$MgCO_3{\cdot}3H_2O + CaCO_3{\cdot}H_2O \rightarrow CaMg(CO_3)_2 + 4H_2O \quad (3)$$

Data show that the concurrent slow dissolution of nesquehonite and monohydrocalcite nourish the precipitation of disordered dolomite. However, disordered dolomite nucleation formed during the first hours (nucleation time 3.2 h), as detected by fitting the Raman spectra (see Movie S1 and Figure S4). These results imply that nesquehonite and monohydrocalcite play a critical retarding effect on the formation of disordered dolomite as discussed below.

The precipitation of disordered dolomite from direct transformation of ACMC could also occur as

$$2Ca_{0.5}Mg_{0.5}CO_3{\cdot}nH_2O \rightarrow CaMg(CO_3)_2 + 2nH_2O \quad (4)$$

This simpler reaction mechanism was detected by time-resolved Raman spectroscopy (Figure 3, experiment 1 in Table 1), but with a low experimental reproducibility (once over four total experiments performed under identical conditions, experiments 1−4 in Table 1). In this particular case, the lifetime of ACMC was larger and equal to 10 h, as shown in Figure 3. Herein, the particle size distribution of disordered dolomite was more homogeneous with an average size of 20 nm (see FESEM images in Figure S2 for experiment 1). We assumed that, in this particular case, ACMC reached an ideal Mg/Ca ≈ 1 ratio and then its direct transformation into disordered dolomite could take place, as demonstrated by the Raman data (Figure 3). However, this chemical event might be strongly sensitive to small fluctuations of room temperature, fluid chemistry, mechanical agitation, and time of mixture of ionic solutions because it happened only once over the four experiments performed under the same conditions (experiments 1−4 in Table 1).

In natural open systems oversaturated with respect to dolomite, fluid chemistry and temperature fluctuations could

https://dx.doi.org/10.1021/acs.cgd.9b01005
Cryst. Growth Des. 2020, 20, 1434−1441

inhibit dolomite formation and the precipitated transient phases could remain persistent and stable for long durations (e.g. refs 28 and 29). Such observations may provide an explanation why dolomite is absent in natural systems presently oversaturated with respect to dolomite.

3.2. Role of Mg Molar Fraction. Under the investigated carbonate alkaline conditions (HCO_3^-/CO_3^{2-} = 1, 0.5 M for each species, and pH ≈ pK_{a2} ≈ 10.3), both the concentration of Mg and its molar fraction with respect to Ca play a critical role in the lifetime of ACMC. When the Mg molar fraction is larger than 0.5, the ACMC lifetime increases substantially (Figure 4). The reaction mechanism, i.e. the nature of transient

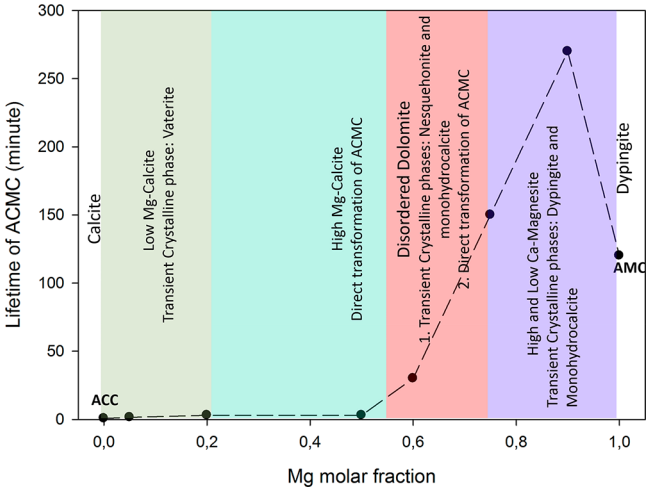

Figure 4. Lifetime of ACMC determined from time-resolved Raman measurements as a function of Mg molar fraction. Eight precipitation experiments were performed with an initial alkaline solution (HCO_3^-/CO_3^{2-} molar ratio = 1, and 0.5 M) at room temperature. Definitions: ACC, amorphous calcium carbonate; ACMC, amorphous calcium−magnesium carbonate; AMC, amorphous magnesium carbonate.

crystalline phases and final recovered products, is also strongly dependent on the concentration of Mg (see Table 1). For example, when the Mg molar fraction is less than or equal to 0.2, the vaterite polymorph is the main transient phase before the formation of low Mg calcite ($Mg_xCa_{1-x}CO_3$ with $x < 0.1$) (Figure S5). Here, three reaction steps are clearly identified: (1) ACC formation with a lifetime of 3 min, (2) concurrent transformation of ACC into vaterite and Mg calcite, and (3) slow transformation of vaterite into low Mg calcite via a coupled dissolution−crystallization process. This reaction mechanism is in agreement with results obtained from in situ time-resolved synchrotron-based wide-angle X-ray scattering (WAXS) and energy dispersive X-ray diffraction (ED-XRD), despite the difference in pH and Mg concentrations.[30] At higher Mg molar fractions (e.g., 0.5 and 0.6), high Mg calcite mesocrystals ($Mg_xCa_{1-x}CO_3$ with $0.1 < x < 0.45$) form and the vaterite phase is not detected (see Table 1). Mg calcite mesocrystals are micrometric porous aggregates constituting oriented nanocrystals that form cauliflower- and peanut-like morphologies (Figure S6). These peculiar morphologies and the process of aggregation of nanocrystals have been reported in previous studies (e.g. refs 22 and 23). In some studies, high Mg calcite with peculiar morphologies and with Mg content in the crystal lattice (<45%) was misinterpreted as disordered dolomite (e.g. refs 15 and 16). Therefore, Mg calcite mesocrystals are not necessarily made of disordered dolomite, except when the Mg/Ca ratio of the crystal lattice is close to 1.

At a Mg molar fraction of 0.75 and under abiotic conditions, we observed the formation of disordered dolomite ($CaMg(CO_3)_2$), as discussed in section 3.1. As complementary support, X-ray data (Figure 5) show the (104) reflection in the

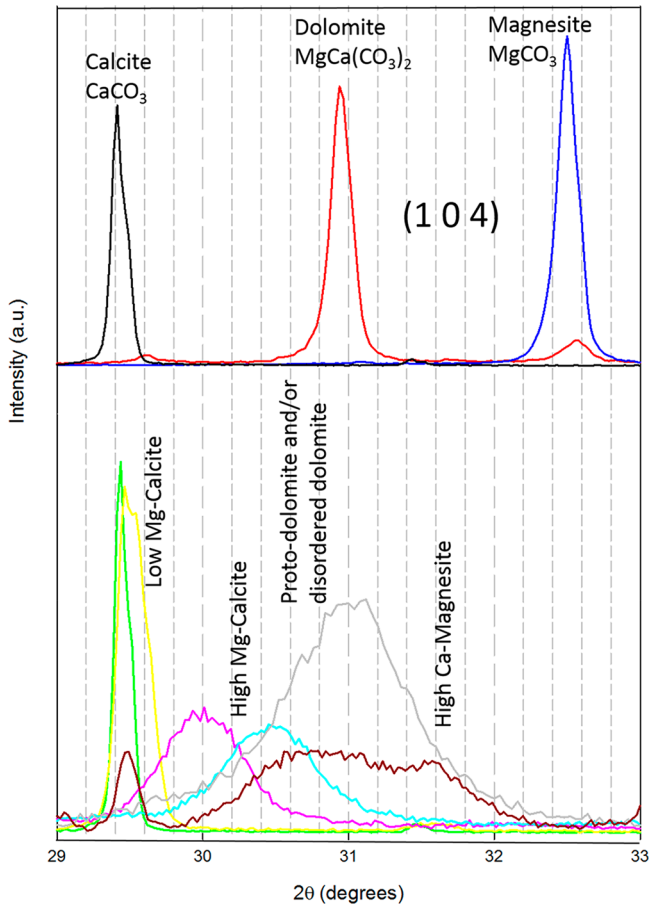

Figure 5. X-ray diffraction data showing the (104) reflection for calcite, dolomite, and magnesite references[13] and solids obtained for different initial Mg molar fractions in solution (0.05, green; 0.2, yellow; 0.5, pink; 0.6, cyan, 0.75: gray, 0.9, dark red), corresponding to experiments 6−10 in Table 1, respectively.

solid products recovered at the end of experiments that used different initial Mg molar fractions (see also Table 1). In addition, from Rietveld refinements of XRD patterns, Table 2 summarizes the mineral composition and Mg content in the calcite crystal lattice. In general, our results are in agreement with studies that have investigated the influence of Mg molar fraction on the lifetime of ACC and ACMC phases and their transformation into crystalline phases (e.g. refs 28−30). In addition to already published studies, our study reports specific experimental conditions that allow the synthesis of disordered dolomite by controlling exclusively the Mg molar content (0.75) and the carbonate alkalinity (HCO_3^-/CO_3^{2-} = 1, pH ≈ pK_{a2} ≈ 10.3) at room temperature (experiments 1−4 in Table 1).

Finally, for a Mg molar fraction of 0.9 (experiment 10 in Table 1), the lifetime of ACMC was prolonged to about 4.5 h and a more complex reaction mechanism was monitored by time-resolved Raman spectroscopy (Figure 6). In this experiment, monohydrocalcite ($CaCO_3·H_2O$) was detected

https://dx.doi.org/10.1021/acs.cgd.9b01005
Cryst. Growth Des. 2020, 20, 1434−1441

Table 2. Mineral Carbonate Composition and Mg Content in Lattice Structure Identified from Rietveld Refinement of X-ray Diffraction Patterns[a]

expt	Mg molar fraction	calcite	low Mg calcite	high Mg calcite	disordered dolomite	high Ca magnesite
5	0	$CaCO_3$	none	none	none	None
6	0.05	$CaCO_3$	none	none	none	none
7	0.20	$CaCO_3$	$Mg_{0.05}Ca_{0.95}CO_3$	none	none	none
8	0.50	none	none	$Mg_{0.15}Ca_{0.85}CO_3$, $Mg_{0.23}Ca_{0.77}CO_3$	none	none
9	0.6	none	none	$Mg_{0.35}Ca_{0.65}CO_3$	none	none
1	0.75	none	none	none	$Mg_{0.49}Ca_{0.51}CO_3$	none
10	0.9[x]	none	$Mg_{0.07}Ca_{0.93}CO_3$	none	$Mg_{0.45}Ca_{0.55}CO_3$	$Mg_{0.68}Ca_{0.32}CO_3$

[a]In experiment 10, aragonite, dypingite, and eteilite were also detected.

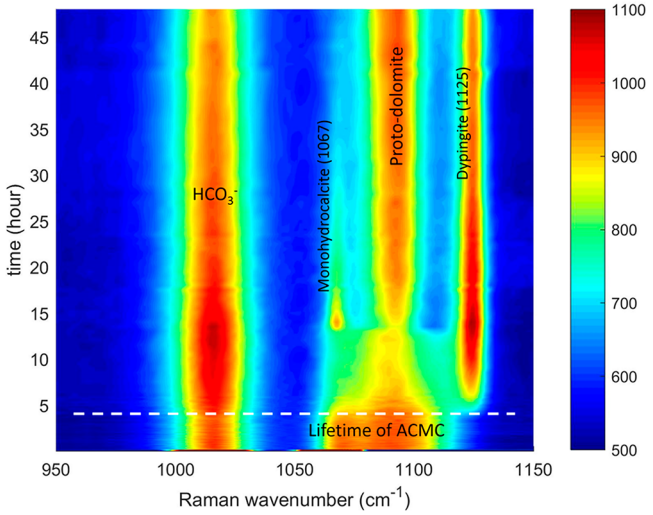

Figure 6. Time-lapse Raman spectroscopy monitoring of the formation of disordered dolomite from ACMC in experiment 10 (Table 1). Monohydrocalcite is a transient phase (Mg molar fraction of 0.9), and dypingite (hydrated Mg carbonate mineral: $Mg_5(CO_3)_4(OH)_2{\cdot}5H_2O$) coexists with disordered dolomite until the end of the experiment.

as a transient phase before the formation of disordered dolomite and high Ca magnesite was measured by X-ray diffraction in the product recovered after the experiment (Figure 5 and Table 2). Dypingite ($Mg_5(CO_3)_4(OH)_2{\cdot}5H_2O$) was also detected, and this hydrated carbonate coexisted with disordered dolomite and Ca magnesite until the end of the experiment (Figure 6). These results demonstrate that the Mg molar fraction controlled the lifetime of ACMC in the interacting solutions, the reaction mechanism, the kinetics, and the amount of Mg incorporated into the carbonate.

4. DISCUSSION AND CONCLUDING REMARKS

Dolomite is a critical mineral that incorporates large volumes of carbon dioxide into a solid form in many geological environments.[1] Primary dolomite formation ($Mg^{2+} + Ca^{2+} + 2CO_3^{2-} \rightarrow CaMg(CO_3)_2$) at low temperature (20−35 °C) and secondary dolomite formation ($2CaCO_3 + Mg^{2+} \rightarrow CaMg(CO_3)_2 + Ca^{2+}$) at higher temperature (diagenetic or hydrothermal, 60−300 °C) have been proposed to explain dolomitization processes in natural environments.[1] Primary dolomite formation has led to controversial claims because ordered dolomite could not be synthesized in the laboratory under abiotic conditions and only disordered dolomite and high Mg calcite are generally observed in environments oversaturated with respect to dolomite.[2,15−17] Bioassisted primary dolomite formation and/or formation mediated by living organisms have been proposed. In such cases, cellular and intracellular surfaces and exopolymeric substances can overcome the kinetic barrier to nucleate dolomite (e.g. refs 6−12). Functionalized organic molecules/surfaces can also decrease the Mg hydration barrier and catalyze dolomite formation at low temperature (e.g. ref 31). However, the reaction mechanism responsible for dolomite formation (e.g., role of transient amorphous or crystalline phases) and clear proofs or explanations concerning the dolomite superstructure-ordering reflections in the X-ray diffraction patterns have been ambiguously provided.[6,12] On the basis of the present study and on recent mechanisms proposed to explain mineral nucleation (e.g. refs 32−36), we infer that primary dolomite, as initially defined ($Mg^{2+} + Ca^{2+} + 2CO_3^{2-} \rightarrow CaMg(CO_3)_2$), has a very low probability of forming at room temperature in abiotic or biotic systems, i.e. through heterogeneous nucleation (pre-existence of reactive surfaces), and a nonclassical nucleation mechanism is therefore expected. The present study demonstrates that transient amorphous or crystalline phases play a significant role in the formation of disordered dolomite. Such transient phases can decrease the energy barrier under ideal fluid chemistry conditions (e.g., direct transformation of ACMC into disordered dolomite), but they can also retard dolomite precipitation (e.g., via concurrent dissolution of nesquehonite and monohydrocalcite), as demonstrated in the present study (Figures 1−3 and Movie S1). Crystalline phases (e.g., dypingite, monohydrocalcite, aragonite) can produce an inhibiting effect in laboratory experiments or in some natural dolomitic environments.[1] From the present experimental study, we conclude that ACMC accelerates dolomitization in a short interval of Mg molar content (0.6−0.75) at low temperature and the revealed reaction mechanism could exist in natural dolomitic environments such as lagoons, evaporitic settings, or caves.

Another critical point concerning the so-called primary dolomite is the existence of superstructure-ordering reflections in X-ray diffraction patterns (e.g., (101), (015), and (021), Figure S3). Herein, some factors can perturb their unambiguous detection. For example, when the dolomite crystal size is larger than 100 nm and coexisting crystalline phases have a low concentration, X-ray powder diffraction or electron diffraction in TEM allows a clear identification of superstructure-ordering reflections. Conversely, if the dolomite crystal size is on the order of or smaller than 20 nm (Figure S7), the detection of superstructure-ordering reflections is more challenging in X-ray diffraction patterns and by electron diffraction in TEM when nanoparticles are aggregated, despite the ideal Mg content (Ca/Mg ≈ 1) in the structure lattice (Figure S3). In such a case, disordered dolomite, i.e. short-

https://dx.doi.org/10.1021/acs.cgd.9b01005
Cryst. Growth Des. 2020, 20, 1434−1441

range ordered crystallographic structures, is assumed and, in general, longer range ordering is reached with an increase in temperature (corresponding to an increase in the average size of dolomite crystals) as already demonstrated in a previous study.[13] We claim that the detection limit of laboratory X-ray diffraction data when nanoparticles exist (the peaks are broader and have lower intensity and the low intensity of superstructure-ordering reflections) and the difficulty in synthesizing dolomite in laboratory experiments have led to contradictory interpretations on the formation of dolomite at low temperature. From this perspective, the formation of disordered dolomite at low temperature in abiotic systems can be achieved at room temperature. A future challenge would be to determine whether a regular alternation of monolayers of Ca and Mg (perpendicular to the *c* axis) may exist in nanosized dolomitic crystals, which would require developing specific analytical and imaging methods, such as energy filtered transmission electron microscopy combined with electron energy loss spectroscopy.

■ ASSOCIATED CONTENT

Supporting Information

The Supporting Information is available free of charge at https://pubs.acs.org/doi/10.1021/acs.cgd.9b01005.

Table 1 and Figures 1−7 as described in the text (PDF)

Time evolution of the peaks of the main mineral phases during experiment 2 (AVI)

■ AUTHOR INFORMATION

Corresponding Author

German Montes-Hernandez − *Univ. Grenoble Alpes, Univ. Savoie Mont Blanc, CNRS, IRD, IFSTTAR, ISTerre, 38000 Grenoble, France;* orcid.org/0000-0002-8655-6530; Email: german.montes-hernandez@univ-grenoble-alpes.fr

Authors

François Renard − *Univ. Grenoble Alpes, Univ. Savoie Mont Blanc, CNRS, IRD, IFSTTAR, ISTerre, 38000 Grenoble, France; The Njord Centre, Department of Geosciences, University of Oslo, 0316 Oslo, Norway;* orcid.org/0000-0002-5125-5930

Anne-Line Auzende − *Univ. Grenoble Alpes, Univ. Savoie Mont Blanc, CNRS, IRD, IFSTTAR, ISTerre, 38000 Grenoble, France*

Nathaniel Findling − *Univ. Grenoble Alpes, Univ. Savoie Mont Blanc, CNRS, IRD, IFSTTAR, ISTerre, 38000 Grenoble, France*

Complete contact information is available at: https://pubs.acs.org/10.1021/acs.cgd.9b01005

Notes

The authors declare no competing financial interest.

■ ACKNOWLEDGMENTS

The authors acknowledge funding from the French National Centre for Scientific Research (CNRS).

■ REFERENCES

(1) Warren, J. Dolomite: occurrence, evolution and economically important associations. *Earth-Sci. Rev.* **2000**, *52*, 1−81.

(2) Deelman, J. C. Breaking Ostwald's rule. *Chemie Der Erde-Geochemistry* **2001**, *61*, 224−235.

(3) Pimentel, C.; Pina, C. M. The formation of the dolomite-analogue norsethite: Reaction pathway and cation ordering. *Geochim. Cosmochim. Acta* **2014**, *142*, 217−223.

(4) Hänchen, M.; Prigiobbe, V.; Baciocchi, R.; Mazzotti, M. Precipitation in the Mg-carbonate system-effects of temperature and CO_2 pressure. *Chem. Eng. Sci.* **2008**, *63*, 1012−1028.

(5) Xu, J.; Yan, C.; Zhang, F.; Konishi, H.; Xu, H.; Teng, H. Testing the cation-hydration effect on the crystallization of Ca-Mg-CO_3 systems. *Proc. Natl. Acad. Sci. U. S. A.* **2013**, *110*, 17750.

(6) Vasconcelos, C.; McKenzie, J. A.; Bernasconi, S.; Grujic, D.; Tien, A. J. Microbial mediation as a possible mechanism for natural dolomite formation at low temperatures. *Nature* **1995**, *377*, 220−222.

(7) Warthmann, R.; Van Lith, Y.; Vasconcelos, C.; Mckenzie, J. A.; Karpoff, A. M. Bacterially induced dolomite precipitation in anoxic culture experiments. *Geology* **2000**, *28*, 1091−1094.

(8) Sanchez-Roman, M.; McKenzie, J. A.; Wagener, A-de-L. R.; Rivadeneyra, M. A.; Vasconcelos, C. Presence of sulfate does not inhibit low-temperature dolomite precipitation. *Earth Planet. Sci. Lett.* **2009**, *285*, 131−139.

(9) Kenward, P. A.; Goldstein, R. H.; Gonzalez, L. A.; Roberts, J. A. Precipitation of low-temperature dolomite from anaerobic microbial consortium: the role of methanogenic Archea. *Geobiology* **2009**, *7*, 556−565.

(10) Deng, S.; Dong, H.; Lv, G.; Jiang, H.; Yu, B.; Bishop, M. E. Microbial dolomite precipitation using sulfate reducing and halophilic bacteria: Results from Qinghai lake, Tibetan Plateau, NW China. *Chem. Geol.* **2010**, *278*, 151−159.

(11) Krause, S.; Liebetrau, V.; Gorb, S.; Sanchez-Roman, M.; Mackenzie, J. A.; Treude, T. Microbial nucleation of Mg-rich dolomite in exopolymeric substances under anoxic modern seawater salinity: New insight into an old enigma. *Geology* **2012**, *40*, 587−590.

(12) Daye, M.; Higgins, J.; Bosak, T. Formation of ordered dolomite in anaerobic photosynthetic biofilms. *Geology* **2019**, *47*, 509−512.

(13) Montes-Hernandez, G.; Findling, N.; Renard, F. Dissolution-precipitation reactions controlling fast formation of dolomite under hydrothermal conditions. *Appl. Geochem.* **2016**, *73*, 169−177.

(14) Vandeginste, V.; Snell, O.; Hall, M. R.; Steer, E.; Vandeginste, A. Acceleration of dolomitization by zinc in saline waters. *Nat. Commun.* **2019**, *10*, 1851.

(15) Liu, D.; Xu, Y.; Papineau, D.; Yu, N.; Fan, Q.; Qiu, X.; Wang, H. Experimental evidence for abiotic formation of low-temperature proto-dolomite facilitated by clay minerals. *Geochim. Cosmochim. Acta* **2019**, *247*, 83−95.

(16) Huang, Y.-R.; Yao, Q.-Z.; Lia, H.; Wang, F.-P.; Zhou, G.-T.; Fu, S.-Q. Aerobically incubated bacterial biomass-promoted formation of disordered dolomite and implication for dolomite formation. *Chem. Geol.* **2019**, *523*, 19−30.

(17) Qiu, X.; Wang, H.; Yao, Y.; Duan, Y. High salinity facilitates dolomite precipitation mediated by Haloferax volcaniiDS52. *Earth Planet. Sci. Lett.* **2017**, *472*, 197−205.

(18) Lippmann, F. *Sedimentary carbonate minerals*; Springer-Verlag: 1973.

(19) Montes-Hernandez, G.; Findling, N.; Renard, F.; Auzende, A.-L. Precipitation of ordered dolomite via simultaneous dissolution of calcite and magnesite: New experimental insights into an old precipitation enigma. *Cryst. Growth Des.* **2014**, *14*, 671−677.

(20) Montes-Hernandez, G.; Renard, F. Time-resolved in situ Raman spectroscopy of the nucleation and growth of siderite, magnesite and calcite and their precursors. *Cryst. Growth Des.* **2016**, *16*, 7218−7230.

(21) Long, X.; Ma, Y.; Qi, L. Biogenic and synthetic high magnesium calcite − A review. *J. Struct. Biol.* **2014**, *185*, 1−14.

(22) Yu, P. T.; Tsao, C.; Wang, C. C.; Chang, C. Y.; Chan, C. C. High-Magnesium Calcite Mesocrystals: Formation in Aqueous Solution under Ambient Conditions. *Angew. Chem.* **2017**, *129*, 16420−16424.

(23) Lenders, J. J. M.; Dey, A.; Bomans, P. H. H.; Spielmann, J.; Hendrix, M. M. R. M.; de With, G.; Meldrum, F. C.; Harder, S.; Sommerdijk, N. A. J. M. High-Magnesian Calcite Mesocrystals: A

Coordination Chemistry Approach. *J. Am. Chem. Soc.* **2012**, *134*, 1367−1373.
(24) Yang, H.; Chai, S.; Zhang, Y.; Ma, Y. A study on the influence of sodium carbonate concentration on the synthesis of high Mg calcites. *CrystEngComm* **2016**, *18*, 157−163.
(25) Romanek, C. S.; Jimenez-Lopez, C.; Navarro, A. R.; Sanchez-Roman, M.; Sahai, N.; Coleman, M. Inorganic synthesis of Fe−Ca−Mg carbonates at low temperature. *Geochim. Cosmochim. Acta* **2009**, *73*, 5361−5376.
(26) Wehrmeister, U.; Jacob, D. E.; Soldati, A. L.; Loges, N.; Hager, T.; Hofmeister, W. Amorphous, nanocrystalline and crystalline calcium carbonates in biological materials. *J. Raman Spectrosc.* **2011**, *42*, 926−935.
(27) Wang, D.; Hamm, L. M.; Bodnar, R. J.; Dove, P. M. Raman spectroscopic characterization of the magnesium content in amorphous calcium carbonates. *J. Raman Spectrosc.* **2012**, *43*, 543−548.
(28) Rodriguez-Blanco, J. D.; Shaw, S.; Bots, P.; Roncal-Herrero, T.; Benning, L. G. The role of Mg in the crystallization of monohydrocalcite. *Geochim. Cosmochim. Acta* **2014**, *127*, 204−220.
(29) Rodriguez-Blanco, J. D.; Shaw; Benning, L. G. A route for the direct crystallization of dolomite. *Am. Mineral.* **2015**, *100*, 1172−1181.
(30) Rodriguez-Blanco, J. D.; Shaw, S.; Bots, P.; Roncal-Herrero, T.; Benning, L. G. The role of pH and Mg on the stability and crystallization of amorphous calcium carbonate. *J. Alloys Compd.* **2012**, *536S*, S477−S479.
(31) Roberts, J. A.; Kenward, P. A.; Fowle, D. A.; Golstein, R. H.; Gonzalez, L. R.; Moore, D. S. Surface chemistry allows for abiotic precipitation of dolomite at low temperature. *Proc. Natl. Acad. Sci. U. S. A.* **2013**, *110* (36), 14540−14545.
(32) Gebauer, D.; Völkel, A.; Cölfen, H. Stable prenucleation calcium carbonate clusters. *Science* **2008**, *322*, 1819−1822.
(33) Dideriksen, K.; Frandsen, C.; Bovet, N.; Wallace, A. F.; Sel, O.; Arbour, T.; Navrotsky, A.; De Yoreo, J. J.; Banfield, J. F. Formation and transformation of a short range ordered iron carbonate precursor. *Geochim. Cosmochim. Acta* **2015**, *164*, 94−109.
(34) Gower, L. B.; Tirrell, D. A. Calcium carbonate films and helices grown in solution of poly (aspartate). *J. Cryst. Growth* **1998**, *191*, 153−160.
(35) Gebauer, D.; Kellermeier, M.; Gale, J. D.; Bergstrom, L.; Colfen, H. Pre-nucleation clusters as solute precursors in crystallization. *Chem. Soc. Rev.* **2014**, *43*, 2348−2371.
(36) Wang, T.; Cölfen, H.; Antonietti, M. Nonclassical crystallization: Mesocrystals and morphology change of $CaCO_3$ crystals in the presence of a polyelectrolyte additive. *J. Am. Chem. Soc.* **2005**, *127*, 3246−3247.

https://dx.doi.org/10.1021/acs.cgd.9b01005
Cryst. Growth Des. 2020, 20, 1434−1441